

# Modelling Stellar Irradiances I: the transition regions of FGKM stars

E. Deliporanidou,<sup>\*</sup> G. Del Zanna

*DAMTP, Centre for Mathematical Sciences, University of Cambridge, Wilberforce Road, Cambridge, CB3 0WA, UK*

Accepted XXX. Received YYY; in original form ZZZ

## ABSTRACT

We employed advanced ionisation equilibrium models that we developed in Dufresne et. al. (2024), which include charge transfer and density effects, to model UV stellar irradiances for a sample of stars. Our sample includes  $\epsilon$  Eridani (K2 V),  $\alpha$  Centauri A (G2 V), Procyon (F5 V) and Proxima Centauri (M5.5 Ve). We measured line fluxes from STIS datasets and used O IV and O V as density diagnostics to find the formation pressure of ions in the transition region (TR) and adopted a simple Differential Emission Measure (DEM) modelling. Our findings indicate significant improvements in modelling spectral lines from anomalous ions such as Si IV, C IV and N V of the Li- and Na-like sequences, which produce the strongest lines in the UV. For example, the Si IV lines were under-predicted by a factor of five and now are within 40% the observed fluxes. The improved models allow us to obtain for the first time reliable estimates of some stellar chemical abundances in the TR. We compared our results with available photospheric abundances in the literature and found no evidence for the First Ionisation Potential (FIP) effect in the TR of our stellar sample. Finally, we compared our results with the solar TR that can also be described by photospheric abundances.

**Key words:** stars – irradiances – transition region – stellar abundances – ionisation equilibrium

## 1 INTRODUCTION

This paper is the first in a series where we study XUV stellar irradiances, aiming to improve the atomic data and provide accurate modelling. Measuring XUV stellar irradiances is important for modelling exoplanet atmospheres (see, e.g. Linsky 2019). The EUV has a particular importance, but very few observations of nearby stars are available from low-resolution EUVE spectra. We will discuss the modelling of the EUV in future papers.

In the UV, there are plenty of observations from e.g. the Space Telescope Imaging Spectrograph (STIS), with primarily emission from the chromospheres and transition regions (TR). It is now well known that the TR of the Sun and stars have little variability with the activity cycles (see, e.g. Del Zanna & Andretta 2015; Ayres 2015). However, the modelling of the strongest TR UV lines is notoriously difficult: zero density ionisation equilibrium (the so-called coronal approximation, the standard in astrophysics), in combination with simple emission measure modelling have failed to accurately predict the observed intensities of lines from the ‘anomalous’ ions, those belonging to the Li- and Na-like sequences, such as Si IV, C IV and N V. Such ions produce the strongest emission lines in the UV, which are under-predicted by significant factors (2–5) compared to those from other ions forming at similar temperatures. This problem was observed on the Sun for a long time (see the review by Del Zanna & Mason (2018)). Del Zanna et al. (2002) combined EUV and UV observational data to show for the first time that these anomalous ions are

also under-predicted by large factors in stellar atmospheres of active stars.

Sim & Jordan (2005) developed an approximate ionisation equilibrium by including density and charge transfer effects for a few carbon and silicon ions and applied it, together with simple 1D emission measure analyses, to UV observations of  $\epsilon$  Eridani, which is a K2 V dwarf star. They claimed to have resolved the main discrepancies in the anomalous ions, although close inspection of their results still indicate large deviations for several lines. On the other hand, Judge et al. (1995) also developed improved ionisation equilibrium models similar to those of Sim & Jordan (2005), but did not find significant improvements in the anomalous ions when applying an emission measure modelling to solar irradiances. Their conclusion was that other physical effects are at play.

We also developed advanced ionisation equilibrium models that include density dependent and charge transfer effects with updated atomic rates, and recently made them available to the community via CHIANTI version 11 (Dufresne et al. 2024). We found significant improvements when comparing observed and predicted radiances for a solar plage observation in the UV, considering the same lines regularly observed by HST/STIS. The main differences between the advanced models and the coronal approximation used in the previous CHIANTI versions (Dere et al. 1997; Del Zanna et al. 2021), is that the anomalous ions have increased intensities by factors of 2-5 and the formation temperatures of all TR lines are shifted towards lower values.

The first aim of this paper is therefore to quantify improvements in modelling the lines from anomalous ions in stellar transition regions. We adopt a simple 1D DEM modelling, as common in the literature,

<sup>\*</sup> E-mail: ed650@cam.ac.uk

although we point out that this is an unphysical representation of the whole atmosphere of a star. The second aim is to use these advanced models to derive, to our knowledge for the first time, relative chemical abundances in the transition regions of a sample of stars.

The present paper focuses on STIS UV observations of the transition regions of four stars:  $\epsilon$  Eridani (K2 V),  $\alpha$  Centauri A (G2 V), Procyon (F5 V), and Proxima Centauri (M5.5 Ve). Our stellar sample was chosen to investigate the First Ionisation Potential (FIP) effect in stellar TR. This effect, first seen in the active solar corona (Pottasch et al. 1963), is characterised by an overabundance of low-FIP elements ( $< 10$  eV), such as Fe, Mg and Si compared to high-FIP elements ( $> 10$  eV), such as C, N, O. Telleschi et al. (2005) note that more active, younger stars have a different FIP effect compared to older, less active stars. For a review of the solar literature, where several results turned out to be incorrect, see Del Zanna & Mason (2018). The photospheric composition of the solar TR was noticed in an early study from Laming et al. (1995), and this has been reaffirmed in more recent reviews, such as Del Zanna & Mason (2018). As solar irradiances in the transition region vary little (20-30%) with the solar cycle (Del Zanna & Andretta 2015), the active Sun as a star also has near photospheric abundances in the TR.

Laming (2004) developed theoretical models to explain the physical mechanisms behind the FIP effect, proposing that the enhancement of low-FIP elements occurs due to the ponderomotive force acting on ionised particles in the chromosphere and TR. An explanation for the inverse FIP effects was also put forward. Therefore, the FIP and inverse FIP effects are not just an annoying feature when modelling stellar irradiances, but could in principle be turned into a significant diagnostic tool of stellar magnetic activity and atmospheric dynamics (Laming 2017).

EUV and X-ray observations of the hot plasma in stellar coronae have shown a large variety of results, with both FIP and the opposite, Inverse IFIP (IFIP) effects present among active stars and with variations with stellar activity, see e.g. the reviews by Laming (2015); Seli et al. (2022). To study further the FIP dependence on the stellar activity, Wood & Linsky (2010) compared EM distributions and coronal abundances of seven moderately active dwarfs of different stellar types. They found that the time-dependent interpretation can only be tested if there are multiple observations of the same star at different times. They did find however, a strong correlation of FIP bias with the spectral type, with earlier type stars having solar-like FIP effects and the later stars having inverse FIP effects.

Earlier studies suffered from many limitations. A significant limitation was that stellar coronal abundances were often measured relative to the solar photospheric abundances, whenever stellar measurements were not available. Within the past two decades, a large number of surveys have now provided many stellar photospheric abundances, so the FIP effect can now be properly studied. Another limitation of earlier studies is related to the significant changes in the solar photospheric abundances of key high-FIP elements such as C, N, O.

On the basis of the solar results, we would expect to find chemical abundances close to the photospheric ones in the transition regions of our stellar sample, as stellar TR also tend to vary little (see, e.g. Ayres 2015). To our knowledge, such measurements have not been previously attempted. The advanced models do give us the opportunity to provide such measurements, although for only a few elements.

We detail the methods used in our analysis in Section 2. In Section 3 we describe the observational data, the chosen stellar sample, and the relevant literature, including the available photospheric abundances. In section 4 we present our results that include improved DEM modelling, enhanced line ratios and estimates for the stellar TR

abundances. In section 5 we compare our results with existing photospheric abundance measurements, assessing the FIP effect within our stellar sample and finally compare our findings with solar TR irradiances in the EUV.

## 2 METHODS

To avoid dealing with radiative transfer effects for this initial study, we have chosen optically thin lines and did not consider singly ionised atoms, also for the following reasons: as shown in Dufresne et al. (2021, 2023), singly ionised atoms are also affected by photoionisation which makes the modelling more complex. We have assessed their atomic data and have found that they are often not very accurate. We will discuss these issues and provide improvements in follow-up papers. Our calculations included photoexcitation of the disk radiation (assuming a black-body with the  $T_{\text{eff}}$  of each star), which also affects some low charge states.

We measured line fluxes from STIS datasets (see Table 1) and utilised O IV, O V lines as a density diagnostic. We assumed a constant pressure for ions in the stellar TR, as commonly adopted in the literature (note that radiative transfer calculations for a static atmosphere do indicate constant pressure in the TR). We finally used a pressure of  $10^{16} \text{ cm}^{-3} \text{ K}$  for  $\epsilon$  Eridani, Proxima Centauri, and Procyon and a pressure of  $5 \times 10^{14} \text{ cm}^{-3} \text{ K}$  for  $\alpha$  Centauri A.

We eventually evaluated the improvements in modelling anomalous ions and derived reliable estimates of stellar abundances via a DEM modelling using the CHIANTI\_DEM routine and the default MPFIT option.

Once we obtain the fluxes we can either obtain a volume or a column emission measure. Neglecting interstellar absorption, the flux in an optically thin line of wavelength  $\lambda_{ij}$  (frequency  $\nu_{ji}$ ) from a star at a distance  $d$  is:

$$F(\lambda_{ji}) = \frac{h\nu_{ji}}{4\pi d^2} \int_V N_j A_{ji} dV \quad [\text{erg cm}^{-2} \text{ s}^{-1}] \quad (1)$$

where  $N_j$  is the population of the upper state,  $V$  is the emitting volume, and  $A_{ji}$  is Einstein's A-value. The relation is usually written as:

$$F(\lambda_{ji}) = \frac{1}{d^2} \int_V Ab G(T, N_e) N_e N_H dV \quad (2)$$

where  $Ab$  is the elemental abundance,

$N_e N_H$  the electron and neutral hydrogen number densities, and  $T$  is the electron temperature.  $G$  is the contribution function of the line calculated by the CHIANTI programs, in  $\text{erg cm}^3 \text{ s}^{-1} \text{ sr}^{-1}$ :

$$G(N_e, T) = A_{ji} \frac{h\nu_{ij}}{4\pi} \frac{N_j(Z^{+r})}{(Z^{+r})} \frac{N(Z^{+r})}{N(Z)} \frac{1}{N_e} \quad (3)$$

where  $N_j(Z^{+r})/N(Z^{+r})$  is the population of the upper level  $j$ , relative to the total ion population,  $N(Z^{+r})/N(Z)$  is the ion abundance, calculated with the advanced v.11 model.

Assuming that there is a single relation between the densities and the electron temperature, one defines a volume DEM as

$$DEM_V = N_e N_H dV/dT \quad [\text{cm}^{-3} \text{ K}^{-1}].$$

Our choice here is instead to assume spherical symmetry, i.e. that the stellar emission comes from  $dV = 4\pi r^2 dh$ , so we have

$$F(\lambda_{ji}) = \frac{4\pi r^2}{d^2} \int_T Ab G(T, N_e) DEM(T) dT \quad (4)$$

by assuming that a single-valued column DEM exists:

$$DEM(T) = N_e N_H dh/dT \quad [\text{cm}^{-5} \text{ K}^{-1}].$$

**Table 1.** Stellar Parameters and Observational Data for the four active dwarf stars

Star name	Type	STIS dataset	Date	$T_{\text{eff}}$ [K]	Distances [pc]	Radius [R/R <sub>⊙</sub> ]	Pressure [cm <sup>-3</sup> K]
ε Eridani	K2 V	O55P01030	2000-03-17	5180	3.22	0.74	1 × 10 <sup>16</sup>
A Centauri A	G2 V	O53P01030	1999-02-12	5770	1.34	1.23	5 × 10 <sup>14</sup>
Procyon	F5 1V	OBKK13040	2011-04-05	6704	3.51	2.05	1 × 10 <sup>16</sup>
Proxima Centauri	M5.5 Ve	O5EO01010	2000-05-08	3050	1.29	0.15	1 × 10 <sup>16</sup>

In this way, we can compare the DEM values among the different stars and the Sun, as we know their distance and radius. Note that in the literature the emission measures, which are the integral in temperature bins of the DEM are often presented. Also, often the DEM is defined as  $DEM(T) = N_e^2 dh/dT$ .

We used the Fontenla et al. (2014) facula model atmosphere for all stars to calculate charge transfer for the ion balances, as its pressure through the TR aligns well with the pressures derived from the observations.

When reviewing the literature on photospheric measurements, we encountered several issues. First, different methods and choices of atoms / lines normally produce different results. Second, significant variations (30–50%) are found in the literature results. Third, since measurements are normally reported as relative to solar abundances, the uncertainty in the solar values is an additional factor. We have chosen as reference the latest solar photospheric values by Asplund et al. (2021), noting that the abundances of elements such as C,N,O are significantly (more than 30%) different from the values used in the earlier literature. Nevertheless, we point out that the FIP bias has values that typically range between 2 and 4, so the cited uncertainties in the photospheric abundances do not affect the main results shown here.

To address these challenges, we carefully analysed the photospheric abundances for each star via our DEM analysis. The DEM provides a measure of the distribution of emitting plasma at different temperatures in the stellar atmosphere but can also serve as a diagnostic tool for measuring elemental abundances using spectral lines (Del Zanna & Mason 2018).

We specifically chose the best fit of the DEM while varying elemental abundances for all stars. By applying the advanced models, we investigated discrepancies between the various abundance values reported in the literature. Given the improvements observed in the transition region modelling of the Sun (Dufresne et al. 2024), we trusted these models to provide a measure of the relative abundance values for each star. This selection was also based on achieving the best predicted-to-observed flux ratio.

### 3 DATA

#### 3.1 Observational Data

The datasets for all four stars were obtained from STIS, using either the E140H or E140M gratings, and within the primary wavelength range of  $1100 < \lambda < 1700$ . We used the recently (December 2023) reprocessed STIS data from the MAST website, which provides an uncertainty measurement for each pixel in the data.

Our selection was based on the longest exposure times and the dates, choosing datasets closer to the launch date of the instrument to minimise potential degradation effects. Additionally, an important criterion was the availability of Chandra LETG datasets for the same observational dates to extend our analysis to X-Ray spectra in future

papers and further investigate the FIP effect in the coronae of these stars.

Details such as dataset names and observation times, along with essential parameters for each stellar object, are provided in Table 1. Our analysis showed minor differences between the E140H and E140M gratings.

The line fluxes were obtained with the *cfits* package, developed by S.V.Haughan for SOHO, and custom-written programs. We applied a rebinning factor of 2 to enhance the signal-to-noise ratio, and removed a background. The fitting assumed Gaussian line profiles, which is very accurate for most cases. We calculated the effective temperature ( $T_p$ ) as the average of the temperature, weighted by the product of the line contribution function,  $G(T)$ , with the DEM:

$$\log T_p = \frac{\int G(T) DEM(T) \log T dT}{\int G(T) DEM(T) dT} \quad (5)$$

We have also compared the line fluxes with those obtained by summing the signal over the entire line profile, removing a background, along the lines of Ayres (2015). We found minor differences, of the order of a few percent, between the two methods, for the stronger lines. We have also compared our results to any available in the literature, finding small differences, typically within 10%.

In addition, we closely looked at strong lines such as the C III multiplet lines to make sure that the wavelengths of the lines were at rest for the fitting (as we are not interested in measuring Doppler shifts). We found that A Cen A was blue-shifted by  $\lambda = 0.1 \text{ \AA}$ , and ε Eridani was blue-shifted by  $\lambda = 0.8 \text{ \AA}$ .

#### 3.2 Atomic Data and line selection

We have used data from the latest CHIANTI v.11 release, (Dufresne et al. 2024). For UV emissions, interstellar absorption is a significant problem below 912 Å, where the ISM is opaque due to strong absorption by neutral hydrogen. Above 912 Å, while there is still absorption (notably around specific lines like the Lyman-alpha 1216 Å line), the ISM becomes more transparent, allowing for more effective observations of UV emissions from astronomical sources.

In addition, there are blended or self-absorbed lines like the 1526.7 Å Si II, 1404 Å Si IV and O IV as well as the 1334.53 Å and 1335.7 Å C II. We also found that the C II lines were completely non-Gaussian. When fitting the lines, we also included a few nearby neutral lines around the 1401 Å O IV line, as observed in the IRIS spectra, to increase the accuracy of the obtained flux values. However, we did not include any neutral ions in the actual DEM model.

To measure the electron densities, we considered all the O IV multiplet lines, but used the ratio of the  $\lambda = 1401 \text{ \AA}$  and  $\lambda = 1407 \text{ \AA}$  O IV lines, as the 1404 Å is blended, and the 1399 Å is often very weak and tends to indicate lower densities, when used in conjunction with the 1401 Å line, as we found in the solar case (Rao et al. 2022).

We have also considered the O V 1218 vs. 1371 Å line ratio, although it has some temperature dependency. To obtain the pressures,

**Table 2.**  $\epsilon$  Eridani photospheric abundances available in the literature by Zhao et al. (2002); Allende Prieto et al. (2004), applied to solar photospheric values by Asplund et al. (2021).

	Zhao 2002	Allende 2004	This work
H	12.00	12.00	12.00
C	8.51	8.22	8.51
N	7.79	-	7.85
O	8.65	8.65	8.68
Mg	7.53	7.52	7.57
Si	7.47	7.50	7.53
S	7.23	-	7.18
Fe	7.34	7.40	7.51
$T_{eff}$ [K]	5104	-	5104

we considered the effective temperature of formation of these ions with the advanced equilibrium models and the emission measure distributions.

### 3.3 Stellar Sample

#### 3.3.1 $\epsilon$ Eri

$\epsilon$  Eridani (K2 V) is a nearby, young, and active dwarf star located at approximately 3.22 pc away.  $\epsilon$  Eridani's UV spectrum has been extensively analysed using the STIS high-resolution spectra, for understanding the ionisation states and abundances of various elements in its atmosphere.

Jordan et al. (1987) conducted early UV studies using the International Ultraviolet Explorer (IUE) and found strong emission lines indicative of significant chromospheric heating. Sim & Jordan (2005) addressed the issue of the anomalous ions by presenting new ionisation balance calculations for carbon and silicon, with an approximate treatment of dielectronic recombination (DR) suppression and charge transfer (CT). Ness & Jordan (2007) focused on the coronal properties using X-ray observations. They found no difference between photospheric and coronal abundances for a few elements.

We reviewed the literature and found that Zhao et al. (2002) and Allende Prieto et al. (2004) provided accurate metallicities for  $\epsilon$  Eridani. As in many other cases we have looked at, significant variations in the results are found. Also, as usual, measurements are reported as relative to the solar abundances. The resulting  $\epsilon$  Eri photospheric abundances are shown in Table 2. By assessing them, we believe that the Zhao et al. (2002) values are the most reliable to use for our analysis.

Laming et al. (1996) conducted the first coronal abundances analysis of  $\epsilon$  Eridani by analysing EUV spectra, and found some evidence of a solar-like FIP effect. Sanz-Forcada et al. (2004) determined the coronal abundances of four stars including  $\epsilon$  Eridani and reviewed photospheric abundances to investigate the FIP effect. Contrary with Laming et al. (1996), they found a mild FIP-like effect which affects only 2 elements (Ca and Ni), showing a gradual decrease in coronal abundance for elements with increasing FIP. In addition Wood & Linsky (2010) used  $\epsilon$  Eri for a comparison of the EM distributions of seven active dwarfs, based on results from their previous studies (Wood & Linsky 2006). They compared coronal to assumed stellar photospheric abundances and they found a weak FIP effect for  $\epsilon$  Eri, similar to a few more other active stars.

We calculated the pressure of  $\epsilon$  Eridani, using the ratio of the  $\lambda =$

**Table 3.**  $\alpha$  Centauri A photospheric abundances obtained from the literature, Morel et al. 2018, Edvardsson et al. 1993, Buder et al. 2021 (although the N and O abundances are approximated). For the Morel et al. 2018, we used the after GCE abundances.

	Morel 2018	Edvardsson 1993	Buder 2021	Allende 2004
H	12.00	12.00	12.00	12.00
C	8.69	8.62	8.56	8.62
N	8.09	-	7.96	7.83
O	8.88	8.69	8.82	8.94
Na	6.57	6.24	6.71	6.24
Mg	7.85	7.88	8.05	7.99
Al	6.73	6.45	8.87	6.45
Si	7.77	7.51	7.66	7.83
S	7.38	-	7.25	7.12
Ca	6.56	6.50	6.75	6.74
Fe	7.74	7.65	7.75	7.62
Ni	6.51	6.42	6.60	6.42
$T_{eff}$ [K]	5795	5720	5271	5519

1401 Å and  $\lambda = 1407$  Å O IV fluxes as a density diagnostic and found a pressure of  $P_e = 1 \times 10^{16} \text{cm}^{-3} \text{K}$ .

#### 3.3.2 $\alpha$ Centauri A

$\alpha$  Centauri A (also known as Alpha Cen A) is a G2V-type main-sequence star, one of the closest stellar neighbours to our solar system at a distance of approximately 1.34 pc. It forms part of the Alpha Centauri triple star system, which includes Alpha Centauri B and Proxima Centauri.  $\alpha$  Centauri A is a solar like star but slightly larger and more luminous than the Sun, with a mass of about 1.1 solar masses and a radius of roughly 1.2  $R_\odot$ . Despite these differences, many researchers have noted the STIS A Cen A spectrum to be very close to that of the Sun as a star (cf. Pagano et al. 2004).

Pagano et al. (2004) analysed the UV spectrum of Alpha Centauri A, providing measurements of emission line fluxes. They highlighted similarities and differences in UV spectra between Alpha Centauri A and the Sun, noting comparable activity levels but variations in specific line intensities due to differences in magnetic activity and heating mechanisms. Ayres (2015) used high-resolution E140M echelle spectrograms from STIS and studied the FUV emissions of A Cen A. Judge et al. (2004) wanted to determine how A Cen A serves as a proxy for the Sun under intermediate activity conditions, using datasets from STIS. They found similarities in chromospheric line intensities between A Cen A and the Sun under intermediate activity conditions, but slight differences in the TR and coronal emissions. Upon evaluating the fluxes available in the literature and the values we obtained by fitting the lines, we found agreement within 10 % between the published fluxes of Pagano et al. (2004); Ayres (2015); Judge et al. (2004) and ours, if scaled accordingly with the provided scaling factors.

We calculated the pressure of A Cen A using both O IV and O V line fluxes and found that the star is in the low-density limit, hence we used a pressure of  $P_e = 5 \times 10^{14} \text{cm}^{-3} \text{K}$ .

Upon reviewing the literature on photospheric abundances for Alpha Centauri A, we noted that many researchers have used solar photospheric values. We did find specific measured values reported by Morel (2018), Edvardsson et al. (1993), Buder et al. (2021b), and Allende Prieto et al. (2004), which we present on Table 3, scaled to the solar photospheric values by Asplund et al. (2021). Among

these, the best results from our DEM analysis were obtained using the photospheric abundances reported by [Morel \(2018\)](#).

[Raassen et al. \(2003\)](#) analysed Chandra LETG X-ray data for Alpha Cen A and observed that the low FIP elements were more abundant in the star's corona, indicating the presence of an FIP effect. This confirms the initial findings of [Drake et al. \(1997\)](#), who found that the low-FIP elements are overabundant relative to the high-FIP elements by a factor of about 2.

### 3.3.3 Procyon

Procyon (Alpha Canis Minoris) is one of the brightest stars in the night sky and is a binary star system consisting of Procyon A, a F5 IV-V subgiant or main-sequence star, and Procyon B, a faint white dwarf. The system is relatively close to Earth, at a distance of approximately 3.51 pc.

When reviewing the literature for photospheric abundances for Procyon, we found measured values by [Allende Prieto et al. \(2004\)](#); [Buder et al. \(2021a\)](#); [Edvardsson et al. \(1993\)](#); [Drake et al. \(1995\)](#) which we list in table 4. Among these, we found very good results when using the abundances by [Drake et al. \(1995\)](#), which are solar photospheric abundances from [Anders & Grevesse \(1989\)](#), except for iron for which the researchers provide a different value. We list these in table 4 under "This Work". In the same table, we also provide the solar photospheric abundances from [Asplund et al. \(2021\)](#) to highlight the differences, as the solar photospheric composition has changed significantly since 1989. However, we chose to proceed with the abundances from [Drake et al. \(1995\)](#)

Contrary to the solar case, studies by [Raassen et al. \(2002\)](#) and [Schmitt & Ness \(2004\)](#) found a less significant FIP effect for Procyon. [Sanz-Forcada et al. \(2004\)](#) found agreement between photospheric and coronal abundances with a relative underabundance of O in the corona. They also found an indicative abundance trend of a mild FIP bias which increases with temperature in the corona of Procyon, but couldn't confirm the hypothesis due to uncertainties. [Drake et al. \(1995\)](#) also found that the corona of Procyon did not exhibit clear evidence of a solar-like FIP effect and that the observed abundances were all, to within the observational uncertainties, identical to Procyon's photospheric abundances.

We calculated the pressure of Procyon using the ratio of the 1407 Å and 1401 Å O IV lines, finding a high pressure of  $P_e = 10^{16} \text{ cm}^{-3} \text{ K}$ . Under the correct pressure, we would expect the ratio of the calculated-to-observed fluxes of the 1218 Å and 1371 Å O V lines to be consistent. However, the flux ratios of these lines did not agree at  $P_e = 10^{16} \text{ cm}^{-3} \text{ K}$ . Using the 1218 Å and 1371 Å O V lines as density diagnostics, we found a slightly higher pressure of  $P_e = 5 \times 10^{16} \text{ cm}^{-3} \text{ K}$ , although this did not yield good calculated/observed flux ratios for the other ions. Given that Procyon is a quiet star, a high pressure is unexpected, leading us to adopt the initial measurement of  $P_e = 10^{16} \text{ cm}^{-3} \text{ K}$  based on the O IV lines.

### 3.3.4 Proxima Centauri

Proxima Centauri is a red dwarf of spectral class M 5.5, and is part of the Centauri triple stellar system. It is known to have a high level of magnetic activity, which can result in intense flares. It is the closest star to our solar system and the closest known exoplanetary host star candidate ([Lalitha et al. 2020](#)).

Despite finding extensive literature on coronal abundances for Proxima Centauri, actual measurements of its photospheric abundances are lacking. Consequently, we decided to adopt the photospheric abundances of Alpha Cen A from [Morel \(2018\)](#), based on

**Table 4.** Procyon photospheric abundances available in the literature measured by [Buder et al. \(2021b\)](#); [Edvardsson et al. \(1993\)](#); [Allende Prieto et al. \(2004\)](#) and solar photospheric abundances by [Asplund et al. \(2021\)](#) for reference. "This work" consists of abundances used from [Drake et al. \(1995\)](#) except for C and N that are taken from [Anders & Grevesse \(1989\)](#).

	Buder 2021	Edvardsson 1993	This Work	Asplund 2021	Allende 2004
H	12.00	12.00	12.00	12.00	12.00
C	8.44	-	8.56	8.46	8.51
N	7.84	-	8.05	7.83	-
O	8.70	8.64	8.93	8.69	8.67
Na	6.25	6.28	-	6.22	-
Mg	7.61	7.67	7.58	7.55	7.54
Al	6.45	-	-	6.43	-
Si	7.52	7.52	7.55	7.51	7.44
S	7.13	-	7.21	7.12	-
Ca	6.34	6.30	-	6.30	6.70
Fe	7.51	7.58	7.51	7.46	7.49
Ni	6.23	6.24	6.25	6.20	6.27
$T_{eff}$ [K]	6468	6704	6650	-	6677

the assumption that Proxima Centauri, as a member of the Alpha Centauri triple system, shares a similar atmospheric composition due to its formation from the same primordial nebula cloud.

[Fuhrmeister et al. \(2011\)](#) found an inverse FIP pattern during the quiescent state for Proxima Centauri, which aligns with [Lalitha et al. \(2020\)](#) who discussed that an anti-FIP effect is expected during the quiescent emission of moderately active M dwarf stars. [Fuhrmeister et al. \(2022\)](#) anticipated an inverse-FIP abundance pattern for Proxima Centauri based on its stellar type. However, their observations were inconclusive regarding the presence of an FIP or inverse-FIP effect, noting that the abundance pattern was relatively close to solar photospheric values, which could be attributed to the quiescent state of Proxima Centauri during the observations. Similarly, [Güdel et al. \(2004\)](#) identified a rather flat abundance pattern that was also close to solar photospheric values.

We calculated the pressure of Proxima Centauri using the O IV lines and obtained a range of pressures from  $P_e = 10^{16} \text{ cm}^{-3} \text{ K}$  to  $P_e = 5 \times 10^{16} \text{ cm}^{-3} \text{ K}$ , ultimately selecting  $P_e = 10^{16} \text{ cm}^{-3} \text{ K}$  as it provided the most consistent results with our observations.

## 4 RESULTS

After fitting the STIS lines we commenced modelling the DEM for each star. Initially, we examined the contribution functions and removed lines influenced by noise, those that were very weak or those whose atomic data are lacking from the literature. For each star, we carefully reviewed the available photospheric abundances as discussed in Section 3.3. Despite selecting the best available photospheric values, we continued refining the DEM fit, to also be able to accurately determine the presence of the FIP effect in these stellar TRs.

We present our numerical results from the DEM analysis in Table 5, which lists the CHIANTI wavelengths and respective ion identifications for the main lines we used for the DEM analysis, most of which are either anomalous ions, strong emission lines, or significantly influencing the DEM. Although we fit many lines for each star, we provide a representative sample based on the aforementioned criteria. This table includes data for all four stars to facilitate comparison. For each star, we report three key parameters: the formation temperature

**Table 5.** Numerical results of the DEM analysis for all four stars.  $F_{\text{obs}}$  is the measured flux in  $10^{-14}$  erg  $\text{cm}^{-2}$   $\text{s}^{-1}$ .  $\log T_p$  is the effective temperature in [K] and  $\frac{F_{\text{calc}}}{F_{\text{obs}}}$  is the ratio of the calculated/predicted to the observed fluxes.

Wavelength ( $\text{\AA}$ )	Ion	$\epsilon$ Eridani			$\alpha$ Centauri A			Procyon			Proxima Centauri		
		$\log T_p$	$F_{\text{obs}}$	$\frac{F_{\text{calc}}}{F_{\text{obs}}}$	$\log T_p$	$F_{\text{obs}}$	$\frac{F_{\text{calc}}}{F_{\text{obs}}}$	$\log T_p$	$F_{\text{obs}}$	$\frac{F_{\text{calc}}}{F_{\text{obs}}}$	$\log T_p$	$F_{\text{obs}}$	$\frac{F_{\text{calc}}}{F_{\text{obs}}}$
1190.42	Si II	4.05	1.09	0.70	4.13	3.24	0.39	4.17	6.38	0.49	4.16	0.01	1.14
1197.39	Si II	4.06	0.92	0.92	4.13	1.59	0.86	4.19	3.95	0.85	4.19	0.05	0.33
1526.71	Si II	-	-	-	4.07	24.5	0.86	4.11	21.0	1.28	4.09	0.10	0.78
1259.53	S II	4.08	1.25	1.67	-	-	-	4.31	14.2	0.55	4.23	0.06	0.96
1253.81	S II	-	-	-	4.27	2.07	0.73	4.35	9.12	0.63	4.27	0.03	1.62
1335.71	C II	4.27	18.6	1.30	4.35	739	0.99	4.41	317	0.60	4.43	1.13	1.35
1334.53	C II	4.27	45.7	1.05	4.35	17.1	0.84	4.40	499	0.74	4.42	2.58	1.15
1206.51	Si III	4.54	33.1	0.82	4.56	152	0.77	4.57	476	1.11	-	-	-
1323.97	C II	4.62	0.12	1.01	4.60	0.69	0.74	-	-	-	4.74	0.04	0.38
1298.95	Si III	4.63	1.67	0.97	4.63	3.96	0.96	4.62	18.0	1.92	4.65	0.22	1.22
1294.54	Si III	4.63	0.59	0.79	4.64	1.22	0.91	-	-	-	4.65	0.13	0.59
1200.97	S III	4.64	0.64	1.10	4.66	1.96	1.36	4.63	14.3	1.00	4.65	0.12	0.86
1194.02	S III	4.65	0.69	0.62	4.66	1.11	1.51	4.64	7.61	1.17	4.65	0.09	0.74
1296.61	S IV	4.70	0.26	1.42	4.69	0.99	0.88	4.69	4.97	1.60	-	-	-
1175.71	C III	4.77	10.9	1.28	4.75	2.81	1.43	4.76	128	1.30	4.74	1.62	1.27
1175.99	C III	4.77	4.85	0.76	4.75	92.0	1.07	4.77	49.9	0.89	4.74	0.63	0.88
1176.37	C III	4.77	4.00	1.16	4.75	12.8	1.04	4.77	68.7	0.81	4.75	80.8	0.85
1175.26	C III	4.77	3.86	0.97	4.75	10.2	1.04	4.77	38.3	1.16	4.74	0.77	0.72
1174.93	C III	4.77	3.91	1.19	4.76	12.5	1.07	4.77	84.9	0.65	4.74	0.90	0.76
1175.59	C III	4.77	2.89	0.97	4.75	12.7	0.64	4.76	65.0	0.52	4.75	0.74	0.56
1402.77	Si IV	4.82	10.6	0.63	4.79	41.0	0.54	4.79	139	0.80	4.80	0.96	1.02
1393.76	Si IV	4.82	19.9	0.67	4.79	79.4	0.55	4.80	246	0.90	4.80	1.64	1.19
1666.16	O III	4.85	0.58	0.73	4.81	11.1	0.41	4.83	25.2	0.52	-	-	-
1660.80	O III	4.85	1.06	1.01	4.81	22.0	0.52	4.83	54.4	0.60	-	-	-
1416.93	S IV	4.88	0.33	0.72	4.87	0.83	1.16	4.94	7.09	0.23	4.86	0.05	0.62
1486.50	N IV	5.01	0.61	0.69	5.02	4.99	1.04	4.96	32.8	0.17	5.03	0.08	0.52
1406.06	S IV	5.03	0.42	1.26	4.99	1.47	1.05	-	-	-	5.20	0.03	2.41
1404.78	O IV	5.04	0.75	0.64	5.08	4.10	0.95	5.00	23.1	0.46	5.06	0.07	0.70
1399.77	O IV	5.06	0.06	1.02	5.07	1.52	1.02	5.01	13.8	1.01	5.09	0.06	0.77
1407.39	O IV	5.06	0.58	0.94	5.11	1.43	1.05	5.04	13.9	0.98	5.09	0.05	1.06
1401.16	O IV	5.07	1.82	0.98	5.09	9.02	0.90	5.02	48.0	0.90	5.12	0.15	1.05
1199.18	S V	5.09	0.47	1.34	5.11	1.64	1.04	5.05	7.42	1.24	5.15	0.04	1.52
1548.20	C IV	5.18	50.1	1.33	5.15	188	0.91	5.34	668	1.20	5.44	8.95	0.82
1550.77	C IV	5.18	26.8	1.24	5.37	103	0.84	5.34	366	1.10	5.44	4.93	0.75
1218.35	O V	5.43	52.7	1.04	5.37	20.4	0.76	5.51	39.5	1.21	5.49	0.99	1.07
1371.29	O V	5.48	1.12	0.85	5.43	1.60	1.26	5.61	11.3	0.76	5.53	0.20	1.03
1238.82	N V	5.73	8.68	1.19	5.69	24.3	0.81	5.87	103	1.17	5.82	2.87	1.07
1242.80	N V	5.73	4.35	1.19	5.69	13.6	0.90	5.87	55.6	1.08	5.82	1.49	1.03

of each ion, the observed fluxes derived from line fitting, and the ratio of calculated/predicted to observed flux. Following extensive fitting and modelling, we present the best DEM fits for each star in Figure 1, and a combined DEM plot in Figure 2 to allow comparison between the stars and the quiet Sun.

In fig 1 we observed a minimum in the DEM at  $\log T \approx 5.2$  K for all stars (except Procyon, whose minimum point is found at  $\log T \approx 5.4$  K). This is commonly observed, and is related to the radiative losses having a peak in the transition region (TR) emission, as outlined e.g. by Jordan et al. (1987).

In fig 2 we see a comparison of the DEM of all stars in the sample and an old quiet Sun DEM obtained from Skylab, available within the CHIANTI database, derived using the Vernazza & Reeves (1978) average Quiet Sun and a constant pressure of  $P_e = 3 \times 10^{15}$   $\text{cm}^{-3}$  K.  $\epsilon$  Eridani, shown in black, is an active star with a higher level of magnetic activity compared to the Sun, hence it is reasonable to appear higher in the log DEM axis, also suggesting an active corona with substantial high-temperature plasma. A Centauri A, shown in

red, is a solar-like star but slightly older and less active, so the DEM is even lower but pretty close to the Sun and much lower at high temperatures compared to  $\epsilon$  Eridani, again as expected. When it comes to Procyon which is an F-type star, shown in blue, as described earlier we would expect a quiet behaviour, however we see that although the DEM at low temperatures is much lower than the quiet Sun, it remains much higher than all of the stars in the TR, photosphere and chromosphere. This wasn't an expected behaviour, however we also found from the observed irradiances that its pressure is much higher than expected ( $10^{16}$ ) which explains this DEM behaviour. Proxima Centauri is a red dwarf known for its flares, shown in green and shows a similar behaviour to Alpha Centauri A. Last but not least, the DEM of the quiet sun, shown in purple, is relatively low across all temperatures, reflecting less plasma emission compared to the active stars, as expected. It is evident that the Sun's TR can be described by photospheric abundances, as shown in Dufresne et al. (2024).

In general, the DEM is expected to rise after the minimum in temperature which indicates active regions, flares, or other forms

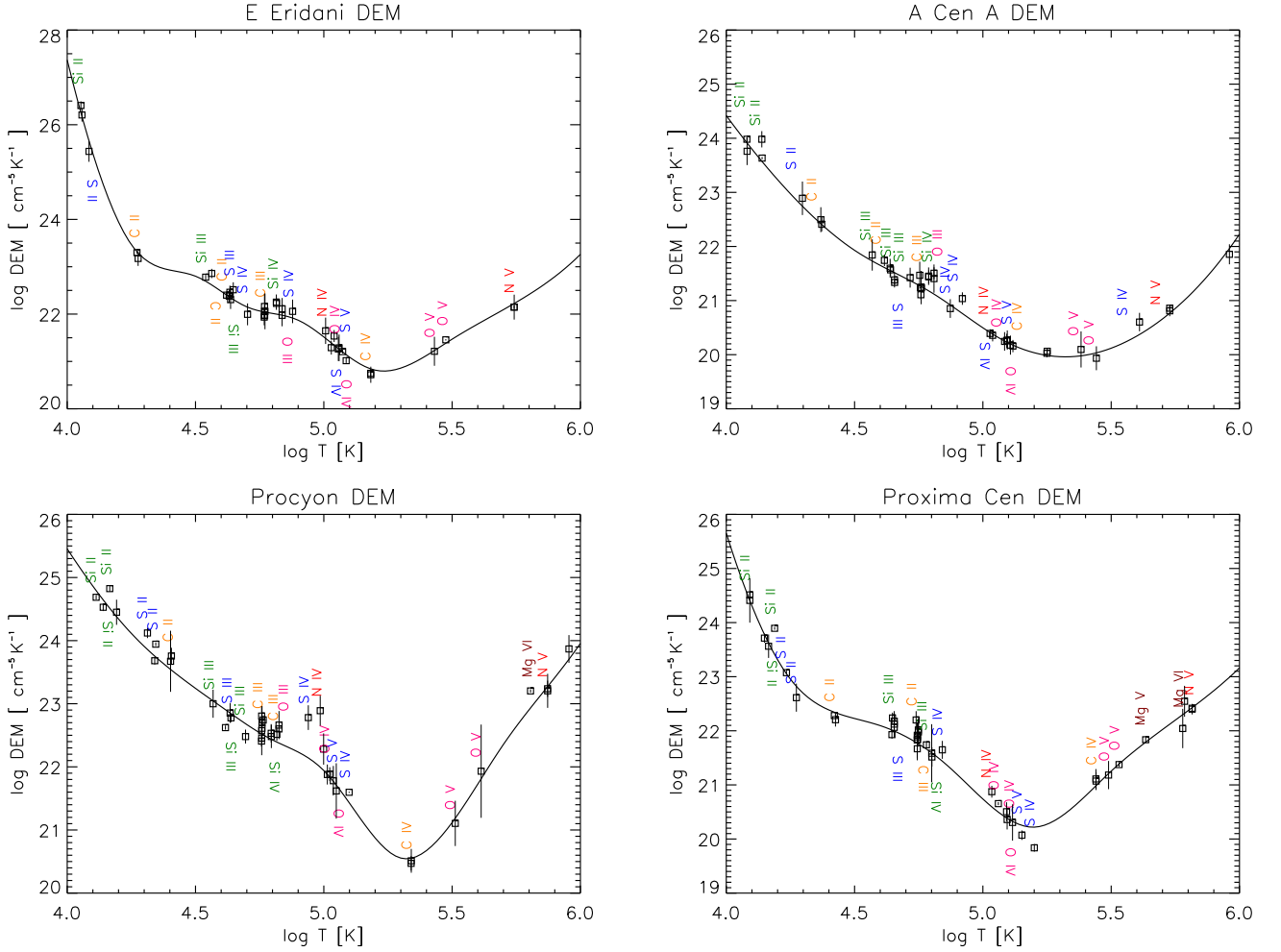


**Figure 1.** DEM plots for  $\epsilon$  Eridani, A Cen A, Procyon, and Proxima Centauri. Different ions are labelled and coloured according to their element.

of coronal heating that contribute to the high-temperature emission. The Quiet Sun and A Centauri A have a slow rise after the minimum, while Procyon, Proxima Centauri and  $\epsilon$  Eridani rise significantly, although observations from other wavelengths need to be considered to constrain the upper TR and the coronae of these stars.

There is plenty of evidence in the solar case that in remote-sensing observations the variations of the S abundance follow those of the high-FIP elements such as Ar, despite this element having FIP = 10 eV (Del Zanna & Mason 2018). The solar S abundance, however, has been uncertain.

For Alpha Cen A we encountered small problems when fitting the lines at 1371 Å (O v), 1402 Å (Si iv), 1238 Å and 1242 Å (N v), and 1501 Å (Si iii). Despite these issues, the overall fitting was consistent with fluxes reported in other studies (Ayres 2015; Judge 2005; Pagano et al. 2004), with a discrepancy of only 10%. Notably, we found no evidence of the FIP effect in the TR of A Cen A, contrary to the findings of Raassen et al. (2003), which suggested its presence in the stellar corona.

For Procyon, the observational data for N iv 1486 Å and S iv were very poor due to significant noise. Therefore, we excluded these lines from the DEM analysis. Similarly to the A Cen A findings, we found that there is no FIP effect in the TR of Procyon. Although Procyon is known as a quiet star, we found an increased DEM (see fig 2)

compared to the rest of the sample, obtained with solar photospheric values.

For Proxima Centauri, we did not find any published results in the literature for modelled UV fluxes to compare with our results. In addition, using the same abundances with A Cen A we found no FIP effect in TR of Proxima Centauri.

For  $\epsilon$  Eridani, we found that the advanced models employed in our study (Dufresne et al. 2024) provide improved calculated-observed flux ratios for some ions, compared to the results obtained with the ionisation balance calculations used by Sim & Jordan (2005). Regarding the FIP effect, our findings indicate an absence of this effect in this star's TR.

In Table 6, we compare the results we obtained with the advanced ionisation equilibrium models with those with the zero-density coronal approximation for  $\epsilon$  Eri as an example of the improvement. The Table also includes a comparison with the results from Sim & Jordan (2005). They present four different models in their paper, but we specifically compare our results with those derived from their simple EMD model (see "M1" in Table 6 below) and their DEMD-A model (see "M2" in Table 6 below), which includes radiative transfer calculations.

In table 6, we present their observed fluxes ( $F_{\text{obs}}$ ) for a few ions, taken from Sim & Jordan (2005) and their  $F_{\text{calc}}/F_{\text{obs}}$  ratio. We note that in most cases, the measured fluxes agree within 10%. For sev-

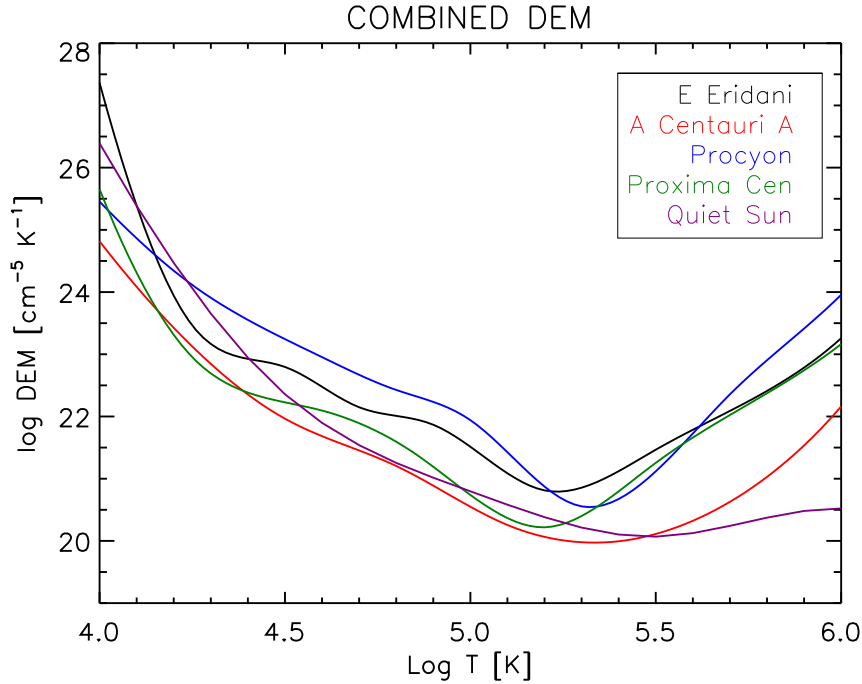


**Figure 2.** Combined DEM plots for  $\epsilon$  Eridani, A Cen A, Procyon, Proxima Centauri, and the quiet Sun.

**Table 6.** Comparison table using  $\epsilon$  Eridani as an example star from the sample. We present three cases: (1) Results from the advanced models in CHIANTI v.11 under "Advanced", (2) results using the coronal approximation under "Coronal", and (3) results from [Sim & Jordan \(2005\)](#). The table includes  $F_{\text{obs}}$  (measured flux in  $10^{-14}$  erg  $\text{cm}^{-2}$   $\text{s}^{-1}$ ) for both our work and [Sim & Jordan \(2005\)](#),  $T_p$  [K] of the ions for the advanced models and coronal approximation, and  $F_{\text{calc}}/F_{\text{obs}}$  for all three cases. "M1" and "M2" under Sim & Jordan 2005 represent the two models we're comparing with, as explained in the text.

Wavelength ( $\text{\AA}$ )	Ion	$F_{\text{obs}}$		Advanced		Coronal		Sim & Jordan 2005	
		This work	Sim & Jordan	$\log(T_p)$	$F_{\text{calc}}/F_{\text{obs}}$	$\log(T_p)$	$F_{\text{calc}}/F_{\text{obs}}$	$\frac{F_{\text{calc}}}{F_{\text{obs}}}$ (M1)	$\frac{F_{\text{calc}}}{F_{\text{obs}}}$ (M2)
1298.95	Si III	1.67	1.67	4.64	0.99	4.74	1.64	0.78	0.80
1294.54	Si III	0.59	0.52	4.64	0.80	4.74	1.33	-	0.73
1402.77	Si IV	10.6	12.1	4.82	0.63	4.92	0.19	0.71	0.64
1393.76	Si IV	19.9	23	4.82	0.67	4.92	0.20	-	0.66
1416.93	S IV	0.33	0.42	4.88	0.83	4.95	0.62	-	-
1486.50	N IV	0.61	0.45	4.99	0.74	5.14	0.47	1.30	1.32
1404.78	O IV	0.75	0.69	5.03	0.68	5.20	0.59	-	-
1399.77	O IV	0.56	0.54	5.05	1.07	5.21	0.83	-	-
1407.39	O IV	0.58	0.52	5.06	0.98	5.21	0.76	-	-
1401.16	O IV	1.82	1.81	5.07	1.03	5.23	0.88	1.89	-
1548.20	C IV	50.1	55.9	5.14	1.33	5.40	0.39	-	0.68
1550.77	C IV	26.8	28.2	5.14	1.24	5.40	0.42	0.81	0.68
1218.35	O V	5.27	6.8	5.40	1.03	5.46	1.36	0.78	-
1371.29	O V	1.12	1.05	5.44	0.81	5.49	1.19	0.60	-
1238.82	N V	8.68	9.4	5.73	1.04	5.79	0.86	0.71	-
1242.80	N V	4.35	4.6	5.73	1.04	5.79	0.86	0.71	-

eral ions, [Sim & Jordan \(2005\)](#) only provide in their Table 7 their calculated flux ratio for the multiplet, which we report in Table 6.

In addition, we note the comparison of the EMDs from the different models that [Sim & Jordan \(2005\)](#) present in their Figure 7. Although they conclude that their DEMD-B is the most favoured, Figure 7 reveals that the EMD of the DEMD-B model is not as smooth as the EMD from the other models that do not show significant improvements in the results.

We measured the stellar TR abundances, using the results of the

DEM analysis. We started as a baseline with the stellar photospheric abundances, and checked if departures were required when doing the fitting. We present our estimates for the stellar TR abundances in Table 7. These estimates were based on groups of ions forming at similar temperatures, ensuring that the ratios of calculated to observed fluxes were consistently accurate. As discussed in the earlier sections, these estimates were derived after reviewing photospheric abundances from the literature which we scaled to solar photospheric values by [Asplund et al. \(2021\)](#) and modelled the DEM using the ad-



**Table 7.** Final estimates of stellar TR abundances for the stellar sample. For  $\epsilon$  Eridani we provide our adjusted TR estimates while the original photospheric values by Zhao et al. (2002) are in parenthesis. For A Centauri A and Proxima Centauri, the values are taken from Morel (2018), and for Procyon we used values from Drake et al. (1995).

	$\epsilon$ Eridani	$\alpha$ Centauri A	Procyon	Proxima Centauri
[Si/C]	0.10 (0.09)	0.12	0.10	0.12
[S/C]	0.05 (0.05)	0.05	0.05	0.05
[S/Si]	0.45 (0.58)	0.41	0.46	0.41
[S/N]	0.21 (0.28)	0.19	0.14	0.19
[S/O]	0.03 (0.04)	0.03	0.02	0.03
[N/C]	0.22 (0.19)	0.25	0.31	0.25

vanced models. For Proxima Centauri, A Centauri A and Procyon we found complete consistency of photospheric values in the TR. For  $\epsilon$  Eridani, we slightly adjusted the photospheric measurements (keeping C fixed) and we provide our adjustments in Table 7 while we also state the original photospheric values by Zhao et al. (2002) in parenthesis. However, we still see consistency of photospheric values in the TR of  $\epsilon$  Eridani, allowing us to conclude that we find no FIP effect in any of the four stellar TR.

## 5 SUMMARY AND CONCLUSIONS

We employed our advanced ionisation equilibrium models (Dufresne et al. 2024) to improve the modelling of four FGKM active stars, A Cen A, Procyon, Proxima Centauri and  $\epsilon$  Eridani. We significantly improved the calculated to observed flux ratios (see Table 5 and Table 6), especially for the anomalous ions, although there are exceptions such as Si IV, which is still under-predicted by up to 40% in one case. We compared our results to those of Sim & Jordan (2005), see Table 6, finding similar results for some ions, but very different for others.

Further improvements could be obtained by e.g. changing the atmospheric model and the amount of neutral hydrogen, as the formation temperature of Si ions is most sensitive to charge transfer effects (cf Dufresne et al. 2024, and references therein).

We evaluated the improvements via a DEM analysis (see fig 1) and compared the results with the quiet Sun (see fig 2). We found that  $\epsilon$  Eridani and Procyon show higher DEM values at high temperatures compared to A Cen A, Proxima Centauri and the quiet Sun, indicating more active and hotter coronae which will be further studied in future papers. The quiet Sun and A Cen A have lower DEM values, showing less emissions at high temperatures, which is characteristic of stars with less magnetic activity. Proxima Centauri, despite being a red dwarf, shows a considerable amount of high-temperature plasma, which is unusual for stars of its type.

From the DEM analysis we also found that the TR of these four stars can well be described by photospheric abundances, contrary to published results on their coronae. For  $\epsilon$  Eridani, we made a small adjustment to the abundances, fixing the C value by Zhao et al. (2002). Our findings are in agreement with our results of the solar TR, where we also found photospheric abundances.

It is somewhat surprising to see such good agreement between predicted and observed fluxes in TR lines, given the very simplistic 1-D DEM modelling of a static atmosphere in ionization equilibrium, which clearly does not correspond to reality. However, regardless of how the plasma density is distributed in height and spatial regions within the atmospheres of the stars, ions that are formed at simi-

lar temperatures should have similar emission measures. Our study, given that the advanced ionization equilibrium (Dufresne et al. 2024) significantly improve the atomic modelling in the TR, indicates that we can use the UV lines to provide abundance estimates in the TR, as it has been commonly carried out for stellar coronae in the XUV. The advantage of this type of modelling is that it is direct and does not require radiative transfer calculations.

In the Sun, the FIP effect is prominently observed at high temperatures (above 1 MK) in active regions with strong magnetic field concentrations, while the quiet Sun corona has photospheric abundances. The solar TR has near photospheric abundances. The spatial extent of active regions is relatively small, and further a significant fraction of the solar TR is not physically connected to the corona, as there are plenty of low-lying cool structures in the quiet Sun and in active regions. The TR emission, which is primarily in the UV, likely reflects processes that are distinct from those in the magnetically strong corona. Therefore, extrapolating to solar-like stars, we were expecting to find from UV measurements photospheric abundances in their transition regions. This is indeed what we found, comparing the few relative abundances we obtained with the few photospheric measurements we found in the literature. Despite the variations in the reference solar photospheric values, the scatter of literature values and the uncertainties in our simple models, a FIP effect of a factor of 3–4 is clearly not present in our stellar sample. Consequently, we didn't find any FIP dependence on the spectral type in the TR.

Solar irradiance variations reveal that, while activity cycles are pronounced in the X-rays and EUV, there is minimal variability in the UV and associated TR emission. This relative stability is attributed to the TR's lesser influence by large-scale magnetic events that dominate the corona. This has been discussed in the literature, for example by Ayres (2015) who investigated stellar activity cycles in the solar-like A Cen A. Consequently, this stability indicates that the TR abundances are close to photospheric regardless of the activity cycle of the star.

Clearly, time-dependent ionization and flows can somewhat affect the ion charge state distributions, so there is scope for further improvements in those areas. We also identified ions that could be useful to measure the FIP effect but for which improved atomic data are needed. We are working towards improving the models for singly ionised ions which require inclusion of photo-ionization and recombination into Rydberg states, plus radiative transfer effects. Finally, we will extend the advanced models to stellar coronae. The effects would be smaller than those we have found for the TR, but should be taken into account. We will then revisit the analyses of stellar coronae using XUV spectra for the same sample to further investigate the FIP effect in these stars.

## ACKNOWLEDGEMENTS

ED acknowledges support from STFC (UK) via a studentship (2882461 related to ST/Y509127/1). GDZ acknowledges support from STFC (UK) via the consolidated grants to the atomic astrophysics group at DAMTP, University of Cambridge (ST/P000665/1. and ST/T000481/1).

Data were obtained from the Multimission Archive at the Space Telescope Science Institute (MAST). STScI is operated by the Association of Universities for Research in Astronomy, Inc., under NASA contract NAS5-26555. Support for MAST for non-HST data is provided by the NASA Office of Space Science via grant NAG5-7584 and by other grants and contracts.

**DATA AVAILABILITY**

The data underlying are available on the MAST website: <https://mast.stsci.edu/search/ui/#/hst>. The atomic data are taken from the CHIANTI database: <https://www.chiantidatabase.org>.

**REFERENCES**

- Allende Prieto C., Barklem P. S., Lambert D. L., Cunha K., 2004, *Astronomy and Astrophysics*, 420, 183
- Anders E., Grevesse N., 1989, *Geochimica et Cosmochimica Acta*, 53, 197
- Asplund M., Amarsi A. M., Grevesse N., 2021, *Astronomy and Astrophysics*, 653, A141
- Ayres T. R., 2015, *The Astronomical Journal*, 149, 58
- Buder S., et al., 2021a, *Monthly Notices of the Royal Astronomical Society*, 506, 150
- Buder S., et al., 2021b, VizieR Online Data Catalog, 750, J/MNRAS/506/150
- Del Zanna G., Andretta V., 2015, *Astronomy & Astrophysics*, 584, A29
- Del Zanna G., Mason H. E., 2018, *Living Reviews in Solar Physics*, 15, 5
- Del Zanna G., Landini M., Mason H. E., 2002, *Astronomy and Astrophysics*, 385, 968
- Del Zanna G., Dere K. P., Young P. R., Landi E., 2021, *The Astrophysical Journal*, 909, 38
- Dere K. P., Landi E., Mason H. E., Monsignori Fossi B. C., Young P. R., 1997, *Astronomy and Astrophysics Supplement Series*, 125, 149
- Drake J. J., Laming J. M., Widing K. G., 1995, *The Astrophysical Journal*, 443, 393
- Drake J. J., Laming J. M., Widing K. G., 1997, *The Astrophysical Journal*, 478, 403
- Dufresne R. P., Del Zanna G., Badnell N. R., 2021, *Monthly Notices of the Royal Astronomical Society*, 503, 1976
- Dufresne R. P., Del Zanna G., Mason H. E., 2023, *Monthly Notices of the Royal Astronomical Society*, 521, 4696
- Dufresne R. P., Del Zanna G., Young P. R., Dere K. P., Deliporanidou E., Barnes W. T., Landi E., 2024, CHIANTI – an atomic database for emission lines – Paper XVIII. Version 11, advanced ionization equilibrium models: density and charge transfer effects, [doi:10.48550/arXiv.2403.16922](https://arxiv.org/abs/2403.16922), <http://arxiv.org/abs/2403.16922>
- Edvardsson B., Andersen J., Gustafsson B., Lambert D. L., Nissen P. E., Tomkin J., 1993, *Astronomy and Astrophysics Supplement Series*, 102, 603
- Fontenla J. M., Landi E., Snow M., Woods T., 2014, *Solar Physics*, 289, 515
- Fuhrmeister B., Lalitha S., Poppenhaeger K., Rudolf N., Liefke C., Reiners A., Schmitt J. H. M. M., Ness J. U., 2011, *Astronomy and Astrophysics*, 534, A133
- Fuhrmeister B., et al., 2022, [10.1051/0004-6361/202243077](https://arxiv.org/abs/10.1051/0004-6361/202243077)
- Güdel M., Audard M., Reale F., Skinner S. L., Linsky J. L., 2004, *Astronomy and Astrophysics*, 416, 713
- Jordan C., Ayres T. R., Brown A., Linsky J. L., Simon T., 1987, *Monthly Notices of the Royal Astronomical Society*, 225, 903
- Judge P. G., 2005, *Journal of Quantitative Spectroscopy and Radiative Transfer*, 92, 479
- Judge P. G., Woods T. N., Brekke P., Rottman G. J., 1995
- Judge P. G., Saar S. H., Carlsson M., Ayres T. R., Judge P. G., Saar S. H., Carlsson M., Ayres T. R., 2004, *ApJ*, 609, 392
- Lalitha S., et al., 2020, *Monthly Notices of the Royal Astronomical Society*, 498, 3658
- Laming J. M., 2004, *The Astrophysical Journal*, 614, 1063
- Laming J. M., 2015, *Living Reviews in Solar Physics*, 12, 2
- Laming J. M., 2017, *The Astrophysical Journal*, 844, 153
- Laming J. M., Drake J. J., Widing K. G., 1995, *The Astrophysical Journal*, 443, 416
- Laming J. M., Drake J. J., Widing K. G., 1996, *The Astrophysical Journal*, 462, 948
- Linsky J., 2019, *Lecture Notes in Physics*, Berlin Springer Verlag, 955
- Morel T., 2018, *Astronomy and Astrophysics*, 615, A172
- Ness J.-U., Jordan C., 2007, *Monthly Notices of the Royal Astronomical Society*, 385, 1691
- Pagano I., Linsky J. L., Valenti J., Duncan D. K., 2004, *Astronomy and Astrophysics*, 415, 331
- Pottasch S. R., Pottasch R. S., 1963, *ApJ*, 137, 945
- Raassen A. J. J., et al., 2002, *Astronomy & Astrophysics*, 389, 228
- Raassen A. J. J., Ness J. U., Mewe R., van der Meer R. L. J., Burwitz V., Kaastra J. S., 2003, *Astronomy and Astrophysics*, 400, 671
- Rao Y. K., Del Zanna G., Mason H. E., Dufresne R., 2022, *Monthly Notices of the Royal Astronomical Society*, 517, 1422
- Sanz-Forcada J., Favata F., Micela G., 2004, *Astronomy and Astrophysics*, 416, 281
- Schmitt J. H. M. M., Ness J. U., 2004, *Astronomy and Astrophysics*, 415, 1099
- Seli B., et al., 2022, *Astronomy & Astrophysics*, 659, A3
- Sim S. A., Jordan C., 2005, *MNRAS*, 361, 1102
- Telleschi A., Güdel M., Briggs K., Audard M., Ness J.-U., Skinner S. L., 2005, *The Astrophysical Journal*, 622, 653
- Vernazza J. E., Reeves E. M., 1978, *The Astrophysical Journal Supplement Series*, 37, 485
- Wood B. E., Linsky J. L., 2006, *The Astrophysical Journal*, 643, 444
- Wood B. E., Linsky J. L., 2010, *The Astrophysical Journal*, 717, 1279
- Zhao G., Chen Y. Q., Qiu H. M., Li Z. W., 2002, *The Astronomical Journal*, 124, 2224

This paper has been typeset from a  $\text{\TeX}/\text{\LaTeX}$  file prepared by the author.